


Knockdown of circ-RAD23B inhibits non-small cell lung cancer progression via the miR-142-3p/MAP4K3 axis

Qingyang Zhuang¹ | Zhangzhou Huang² | Wu Zhuang² | Yaping Hong² | Yunjian Huang² 

¹Department of Radiotherapy, Fujian Cancer Hospital & Fujian Medical University Cancer Hospital, Fuzhou, China

²Department of Thoracic Oncology, Fujian Cancer Hospital & Fujian Medical University Cancer Hospital, Fuzhou, China

Correspondence

Yunjian Huang, Department of Thoracic Oncology, Fujian Cancer Hospital & Fujian Medical University Cancer Hospital, No. 420, Fuma Road, Jinan district, Fuzhou, 350004, Fujian, China.
Email: huangyunjian202093@163.com

Funding information

Natural Science Foundation of Fujian Province, Grant/Award Number: 2018J01274

Abstract

Background: The development of non-small cell lung cancer (NSCLC) is associated with the deregulation of circRNAs. The objective of this study was to investigate the effects of circ-RAD23B in NSCLC.

Methods: Circ-RAD23B expression, miR-142-3p and MAP4K3 was detected by qPCR. Cell proliferation was investigated by CCK-8 assay and colony formation assay. Cell migration and invasion were assessed by transwell assay. Angiogenesis ability was assessed by tube formation assay. Cell cycle distribution and cell apoptosis were monitored by flow cytometry. The predicted binding relationship between miR-142-3p and circ-RAD23B or MAP4K3 was verified by dual-luciferase reporter assay. The protein level of MAP4K3 was detected by western blot. Animal models were established to determine the role of circ-RAD23B in vivo.

Results: Circ-RAD23B was shown to be upregulated in NSCLC tissues and cells. Knockdown of circ-RAD23B inhibited proliferation, migration, invasion, angiogenesis and promoted cell cycle arrest and apoptosis in NSCLC cells, and circ-RAD23B knockdown also impeded tumor growth in vivo. Circ-RAD23B acted as miR-142-3p sponge to inhibit miR-142-3p expression and thus enrich the expression of MAP4K3, a target of miR-142-3p. Rescue experiments presented that miR-142-3p inhibition reversed the effects of circ-RAD23B knockdown, and MAP4K3 overexpression abolished the effects of miR-142-3p restoration. In addition, we found that circ-RAD23B knockdown led to decreased phosphorylation expression of ERK1/2, JNK and p38, three key groups of the MAPK signaling pathway.

Conclusions: Circ-RAD23B knockdown inhibited NSCLC development by regulating the miR-142-3p/MAP4K3 axis, which might be associated with the inactivation of the MAPK signaling pathway.

KEYWORDS

circ-RAD23B, MAP4K3, MAPK, miR-142-3p, NSCLC

INTRODUCTION

Lung cancer has long been the leading cause of cancer-related death. Statistical data in 2019 showed that there were 228 150 estimated new cases and 142 670 estimated deaths of lung cancer in the USA, and the number of cases was far greater than other types of cancers.¹ Approximately 80%–85% of lung cancers are pathologically classified as non-small cell lung cancer (NSCLC). It is widely acknowledged that molecular targeted therapy based on various oncogenic

drivers in tumor cells has greatly improved the treatment of patients with advanced NSCLC.² Therefore, it is necessary to identify more oncogenic drivers to seek novel therapeutic targets for NSCLC.

Recently, it has been reported that circular RNAs (circRNAs) act as either oncogenic drivers or tumor suppressors in the development of NSCLC. For example, circRNA 100 146 has been reported to serve as an oncogene in NSCLC promoting NSCLC cell proliferation and invasion.³ Circ_0007385 also functions as an oncogene to promote

NSCLC cell proliferation, migration and invasion in NSCLC tumorigenesis.⁴ CircRNAs can act as endogenous regulators and regulate multiple biological processes in various diseases.⁵ CircRNAs harbor unique loop-closed structures, with high stability and abundance compared to canonical linear isoforms,⁵ suggesting that circRNAs may have considerable diagnostic, prognostic, and therapeutic value in cancers. A growing number of circRNAs have been identified to be differently expressed in tumor tissues with the advance of circRNAs microarray analysis.^{6,7} Circ-RAD23B (hsa_circ_0087862), derived from RAD23B linear transcript, has been shown to be upregulated in NSCLC tissues by a circRNA expression profile.⁷ The deregulation of circ-RAD23B hinted that circ-RAD23B might be involved in NSCLC progression. However, the evidence was insufficient.

MicroRNAs (miRNAs) have been documented to have multiple functions in physiological and pathological processes of cancers.⁸ Post-transcriptional regulation holds the view that circRNAs harbor miRNA response elements (MREs) and sequester miRNA from other targets.^{9,10} MiR-142-3p has been reported to be a tumor suppressor in NSCLC,¹¹ and circ-RAD23B predicted to have MREs with miR-142-3p by bioinformatics. However, it is unclear whether miR-142-3p role is partly mediated by circ-RAD23B in NSCLC, and this needs further exploration.

Mitogen-activated protein kinase kinase kinase 3 (MAP4K3) is a member of the MAP4K family, and the kinases of the MAP4K family are vital regulators of the MAPK signaling pathway.¹² It has been shown that MAP4K3 is highly expressed in NSCLC tissues and closely associated with the recurrence of NSCLC.¹³ Interestingly, miR-142-3p has been predicted to harbor a binding site with MAP4K3 3' untranslated region (3' UTR), suggesting that MAP4K3 might be a target of miR-142-3p. However, their interactions in NSCLC were not addressed in this study.

Our study aimed to address the detailed functions of circ-RAD23B in NSCLC development and provide a new functional mechanism for circ-RAD23B. The establishment of the circ-RAD23B/miR-142-3p/MAP4K3 axis provides new perspectives into the understanding of NSCLC pathogenesis.

METHODS

Tissue specimens

A total of 50 tumor tissues of NSCLC and 25 normal lung tissues (paired with 25 NSCLC tumor tissues) were included in this study, which were collected from Fujian Cancer Hospital & Fujian Medical University Cancer Hospital. All subjects approved the use of these specimens with written informed consent, and the correlation between clinicopathological features (age, gender, tumor size and TNM stage) and circ-RAD23B expression is shown in Table 1. These tissues were treated with liquid nitrogen after excision and preserved at -80°C until use. This study was implemented with the

TABLE 1 Correlation between clinicopathological parameters of NSCLC patients and circ-RAD23B expression

Parameter	Case	Circ-RAD23B expression		p-value
		Low (n = 27)	High (n = 23)	
Age (years)				0.226
≤60	22	14	8	
>60	28	13	15	
Gender				0.395
Female	25	15	10	
Male	25	12	13	
Tumor size				0.022*
≤5 cm	17	13	4	
>5 cm	33	14	19	
TNM stages				0.0003*
I-II	20	17	3	
III	30	10	20	

Abbreviations: TNM, tumor-node-metastasis.

* $p < 0.05$.

approval of the Ethics Committee of Fujian Cancer Hospital & Fujian Medical University Cancer Hospital.

Cell culture

NSCLC cell lines (Bena culture collection, Beijing, China), including H1299 and A549, and human bronchial epithelioid cells (16 HBE; Bena culture collection) were cultured in RPMI-1640 medium (Bena culture collection), F-12 K medium (Bena culture collection), and DMEM (Bena culture collection), respectively, containing 10% fetal bovine saline (FBS; Bena culture collection). Cells were incubated in a 37°C incubator supplemented with 5% CO_2 .

Quantitative real-time PCR (qPCR)

Total RNA isolated from tissues or cells using Trizol reagent (Invitrogen) was examined using ND2000 (Thermo Fisher Scientific). RNA samples were assembled into cDNA using the SuperScript IV first-strand synthesis system (Invitrogen) or using the miRNA first strand cDNA synthesis kit (Vazyme). Next, cDNA was used for qPCR using the SYBR Green Master Mix (Invitrogen). Relative expression was normalized by GAPDH or U6 and calculated using the $2^{-\Delta\Delta\text{CT}}$ method. The primer sequences are listed as follows:

Circ-RAD23B, F: 5'-GTAATTGCAGCCCTGAGAGC-3' and R: 5'-GATGCTGGAGTGATGGATGC-3'; miR-142-3p, F: 5'-TGCGGTGTAGTGTTCCTACTT-3' and R: 5'-CCAGTGCAGGGTCCGAGGT-3'; MAP4K3, F: 5'-AACTTCCCGACAGTGATGGTT-3' and R: 5'-CACCTTGGTGTCCCTTGTCAT-3'; U6, F: 5'-CTCGCTTCGGCAGCACATA TACT-3' and R: 5'-ACGCTTCACGAATTTGCGTGTC-3'; GAPDH, F: 5'-TCGGAGTCAACGGATTTGGT-3' and R: 5'-TTCCCGTTCTCAGCCTTGAC-3';

Cell transfection

To mediate circ-RAD23B knockdown, small interference RNA (siRNA) targeting circ-RAD23B (si-circ-RAD23B-1 and si-circ-RAD23B-2) and its matched negative control (si-NC) were provided by Genepharma. To mediate miR-142-3p restoration or inhibition, miR-142-3p mimic, miR-142-3p inhibitor and their matched negative control (miRNA NC and inhibitor NC) were provided by Ribobio. The pcDNA-MAP4K3 fusion vector (pc-MAP4K3) for MAP4K3 overexpression and its negative control (pc-NC) were provided by Genepharma. The experimental cells were transfected with oligonucleotides or vectors using lipofectamine 3000 reagent (Invitrogen).

Cell counting kit-8 (CCK-8) assay

H1299 and A549 cells with various transfections were seeded into 96-well plates (2000 cells/well) and incubated for 24 h. Then, cells were treated with CCK-8 reagent (Dojindo) for another 2 h. After incubation, cell viability was checked using a microplate reader (Thermo Fisher Scientific) at 450 nm.

Colony formation assay

H1299 and A549 cells with various transfections were seeded into 6-well plates (200 cells/well) and then incubated in a 37°C incubator supplemented with 5% CO₂ for 2 weeks. During tumor growth, the status of colonies was observed every 3 days. Finally, the number of colonies was counted under a microscope (Olympus).

Transwell assay

Transwell chambers (8 μm pores) were precoated with Matrigel (BD Biosciences). H1299 and A549 cells with various transfections were inoculated into 500 μl serum-depleted culture medium and seeded in the upper chambers of the wells, and 800 μl cultured medium supplemented with 10% FBS as a chemoattractant was added into the lower chambers. The plates were placed in a 37°C incubator containing 5% CO₂ and incubated for 24 h. Afterwards, cells that migrated or invaded to the lower surface of membranes were fixed with methanol (Beyotime) and stained with 0.1% crystal violet (Beyotime). The number of cells were counted in three random fields (at a magnification of 100×) using a light microscope (Olympus).

Matrigel tube formation assay

H1299 and A549 cells with various transfections were cultured in the corresponding culture medium, and the supernatant was collected as the conditional medium. The Matrigel (BD Biosciences) was dissolved at 4°C overnight, and 24-well plates were treated with 100 μl of Matrigel. Human umbilical

vein endothelial cells (HUVECs; Gibco) cultured in the tumor-conditioned medium were placed into 24-well plated (4 × 10⁴ cells/well) coated with Matrigel for 12 h. Next, the images were observed using an inverted photomicroscope (Olympus). Tube formation was assessed according to the number of branches using Image J software (NIH). Five different fields in each group were used to count the number of branches, and the results are shown as the means of the values.

Flow cytometry assay

The transfected cells were treated with trypsin, collected and washed with precooling PBS. Then, cells were fixed using 70% ethanol at 4°C overnight. Cells were stained with 0.5 ml propidium iodide (PI)/RNase A solution (Beyotime) at 37°C for 30 min. The red fluorescence was detected by a flow cytometer (Beckman) at the excitation wavelength of 488 nm to investigate cell cycle distribution.

An Annexin V-FITC apoptosis detection kit (Beyotime) was utilized to monitor cell apoptosis. After transfection, cells were digested with trypsin and collected into PBS. Then, cells were suspended in 195 μl Annexin V-FITC binding buffer and next stained with 5 μl Annexin V-FITC solution and 10 μl PI at room temperature for 20 min. The status of cell apoptosis was examined using a flow cytometer (Beckman).

Dual-luciferase reporter assay

The binding site between circ-RAD23B and miR-142-3p was provided using the Circinteractome tool (<https://circinteractome.nia.nih.gov/>). The binding site between miR-142-3p and MAP4K3 3' UTR was provided by the miRcode tool (<http://www.mircode.org/>). The wild-type (WT) sequences and mutant-type (MUT) sequences of circ-RAD23B and MAP4K3 3' UTR were cloned into pmirGLO plasmid (Promega), and recombinant reporter plasmids included WT-circ-RAD23B, MUT-circ-RAD23B, WT-MAP4K3-3'UTR and MUT-MAP4K3-3'UTR. H1299 and A549 cells were cotransfected with miR-142-3p mimic or miRNA NC and reporter plasmid and then incubated for 48 h. Relative luciferase activity was detected using a dual-luciferase reporter assay system (Promega) according to the manufacturer's protocol.

Western blot

Tissues or cells were lysed in RIPA lysis buffer (Beyotime) to extract total proteins. After separation by 12% SDS-PAGE, proteins were transferred onto PVDF membranes (Bio-Rad) and then blocked in 5% skim milk. The membranes were next incubated with the primary and secondary antibodies, including anti-MAP4K3 (#92427; Cell Signaling Technology), antiproliferating cell nuclear antigen (anti-PCNA; ab18197; Abcam), anti-Bcl-2-associated X protein (anti-Bax; ab182733), anti-ERK1/2 (ab17942; Abcam), anti-

p-ERK1/2 (ab223500; Abcam), anti-JNK (AB208035; Abcam), anti-p-JNK (ab76572; Abcam), anti-p38 (ab32142; Abcam), anti-p-p38 (ab178867; Abcam), anti-GAPDH (ab9485; Abcam) and goat-anti rabbit (ab205718; Abcam). The protein signals were detected using an enhanced chemiluminescence system (Beyotime).

Animal models

NSCLC animal models were established in nude mice (Vital River Laboratory Animal Technology Co., Ltd. Beijing, China; Balb/c, $n = 12$, female). A549 cells infected with lentivirus sh-circ-RAD23B (Genepharma) or sh-NC (Genepharma) were subcutaneously inoculated into the right flank of mice ($n = 6$ per group; 2×10^6 cells per

mouse). Tumor volume (length \times width² \times 0.5) was measured using a caliper once a week for 4 weeks. All mice were subsequently sacrificed after anesthesia, and the tumor tissues were excised and used in subsequent assays. These procedures were approved by the Animal Care and Use Committee of Fujian Cancer Hospital & Fujian Medical University Cancer Hospital.

Statistical analysis

Experiments for each assay were conducted three times. All data are presented as mean \pm standard deviation (SD). Student's *t*-test was used for comparison between two groups, and analysis of variance (ANOVA) was used for comparison among multiple groups. Statistical significance was defined

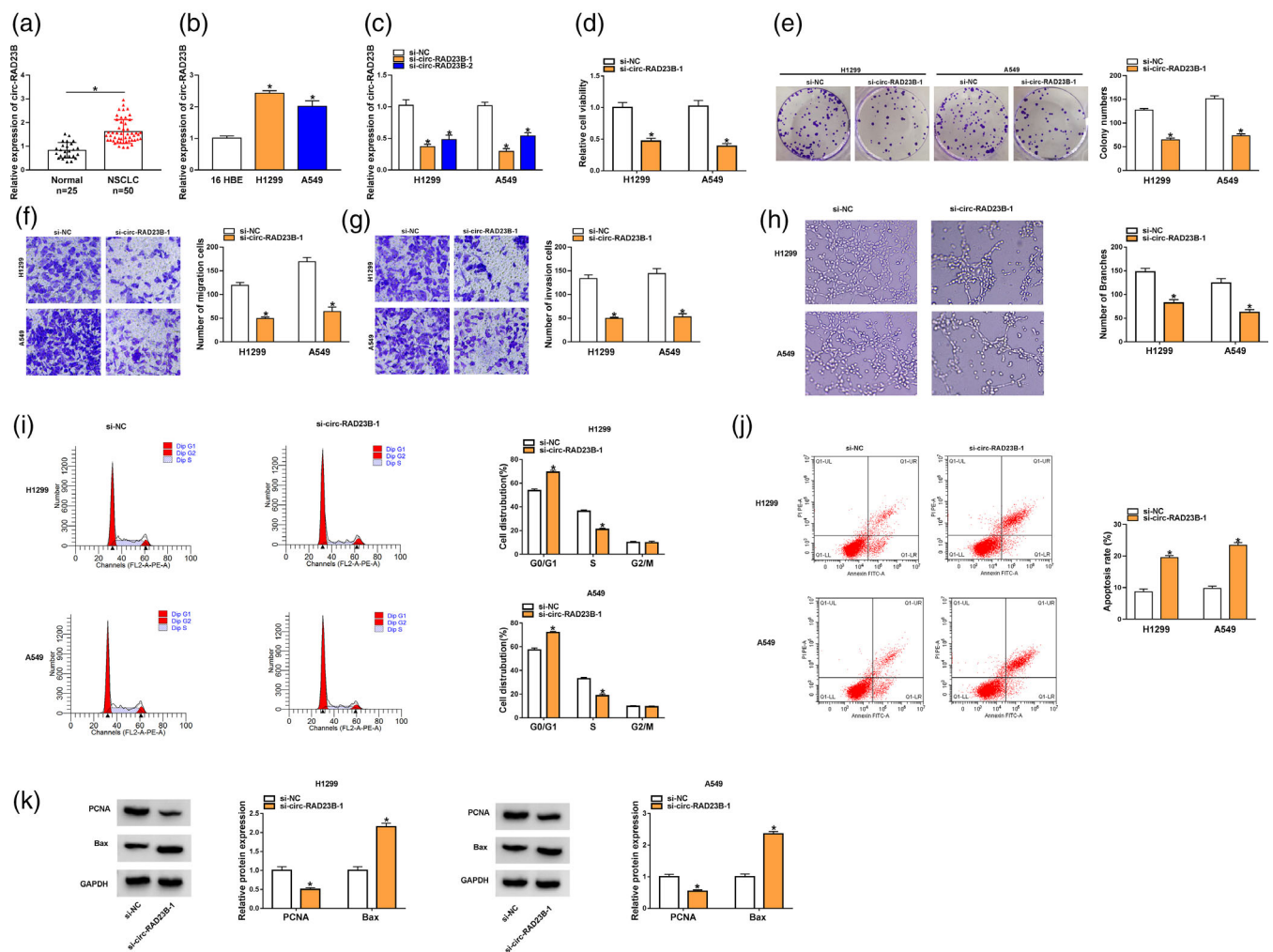


FIGURE 1 Circ-RAD23B knockdown blocked NSCLC development in vitro. (a) The expression of circ-RAD23B in NSCLC tissues and normal tissues was measured by qPCR. (b) The expression of circ-RAD23B in H1299, A549 and 16 HBE cells was detected by qPCR. (c) The efficiency of circ-RAD23B interference was checked by qPCR. (d) The effect of circ-RAD23B knockdown on cell viability was examined by CCK-8 assay. (e) The effect of circ-RAD23B knockdown on cell proliferation was examined by colony formation assay. (f and g) The effect of circ-RAD23B knockdown on migration and invasion was examined by transwell assay. (h) Matrigel tube formation assay was performed to evaluate the angiogenic ability of HUVECs. (i) The effect of circ-RAD23B knockdown on cell cycle distribution was determined by flow cytometry assay. (j) The effect of circ-RAD23B knockdown on cell apoptosis was analyzed by flow cytometry assay. (k) Expression of PCNA and Bax affected by circ-RAD23B knockdown was detected by western blot. * $p < 0.05$

when p -values were less than 0.05. All statistical analysis was performed using GraphPad Prism 7.0 (GraphPad).

RESULTS

Circ-RAD23B knockdown inhibited proliferation, migration, invasion, angiogenesis and promoted cell cycle arrest and apoptosis in NSCLC cells

Circ-RAD23B expression was shown to be increased in NSCLC tissues ($n = 50$) compared to normal tissues ($n = 25$) (Figure 1a). Follow-up analysis manifested that high circ-RAD23B expression (with median value as the cut-off value) was linked to low survival of NSCLC patients ($p = 0.0075$; Figure S1). In addition, circ-RAD23B expression was shown to be elevated in H1299 and A549 cells compared to 16 HBE cells (Figure 1b). Then, we used siRNA targeting circ-RAD23B to reduce the expression level of circ-RAD23B in H1299 and A549 cells. The data presented that circ-RAD23B expression was strikingly decreased in H1299 and A549 cells with si-circ-RAD23B-1 or si-circ-RAD23B-2 transfection (Figure 1c), and si-circ-RAD23B-1 was used in the following assays because si-circ-RAD23B-1 possessed higher efficiency on circ-RAD23B interference. Next, we found that circ-PAD23B knockdown remarkably inhibited H1299 and A549 cell proliferation because of the decreased cell viability and colony formation ability caused

by circ-PAD23B knockdown from CCK-8 assay and colony formation assay (Figure 1d and e). In addition, circ-PAD23B knockdown significantly depleted the properties of cell migration and invasion by transwell assay (Figure 1f and g). Moreover, circ-PAD23B knockdown notably weakened the number of branches in HUVECs after the treatment with the conditioned medium from si-circ-RAD23B-1-transfected H1299 and A549 cells, suggesting that circ-PAD23B knockdown inhibited angiogenesis (Figure 1h). Circ-PAD23B knockdown also induced cell cycle arrest at the G0/G1 phase and promoted cell apoptosis in H1299 and A549 cells (Figure 1i and j). Additionally, we found that circ-PAD23B knockdown weakened the expression of PCNA but promoted the expression of Bax (Figure 1k). The data suggested that circ-RAD23B was aberrantly upregulated in NSCLC cells, and circ-PRD23B knockdown blocked cellular malignant properties.

MiR-142-3p was a target of circ-RAD23B

We subsequently explored the functional mechanism of circ-PAD23B. The data from the Circinteractome tool showed that miR-142-3p was one of the targets of circ-RAD23B, and circ-RAD23B harbored a special binding site with miR-142-3p (Figure 2a). MiR-142-3p mimic introduction in H1299 and A549 cells significantly increased the expression of miR-142-3p (Figure 2b). In dual-luciferase reporter assay, miR-142-3p mimic transfection notably

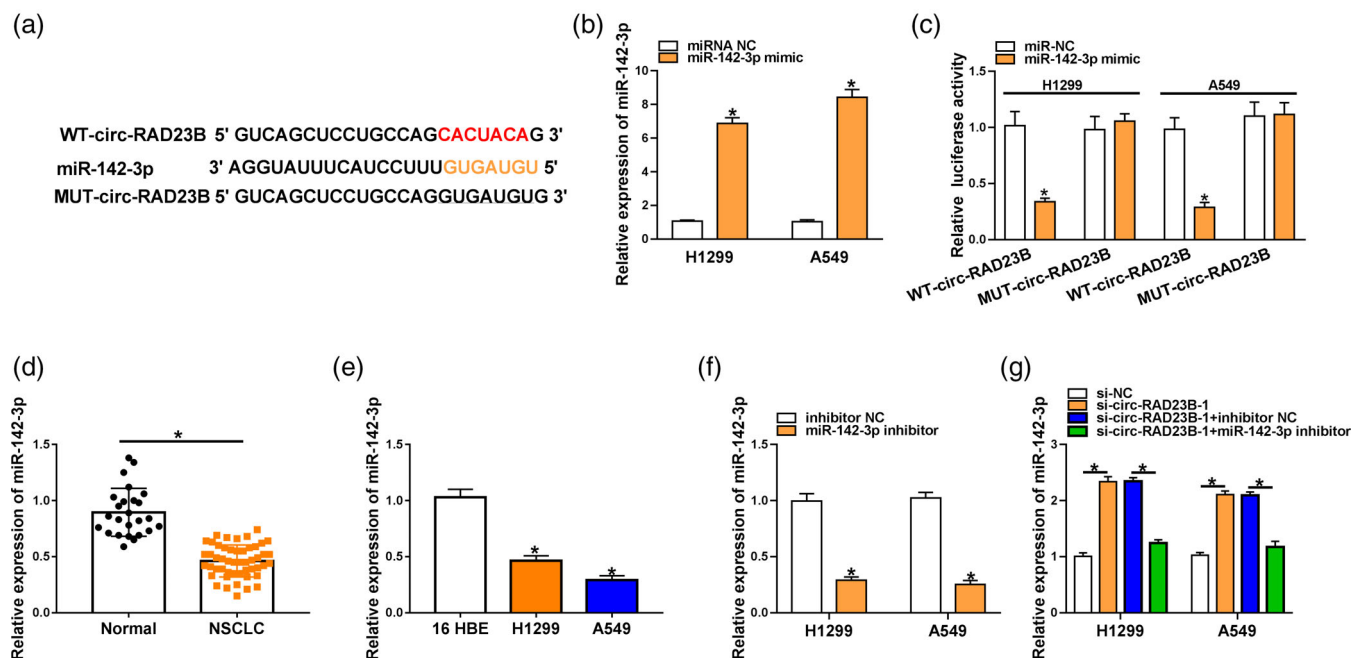


FIGURE 2 MiR-142-3p was a target of circ-RAD23B. (a) the binding site between circ-RAD23B and miR-142-3p was provided by Circinteractome tool. (b) The efficiency of miR-142-3p mimic was examined by qPCR. (c) Dual-luciferase reporter assay was performed to validate the interaction between circ-RAD23B and miR-142-3p. (d) The expression of miR-142-3p in NSCLC tissues and normal tissues was detected by qPCR. (e) The expression of miR-142-3p in H1299, A549 and 16 HBE cells was detected by qPCR. (f) The efficiency of miR-142-3p inhibitor was checked by qPCR. (g) The expression of miR-142-3p in H1299 and A549 cells transfected with si-circ-RAD23B-1 or si-circ-RAD23B-1 + miR-142-3p inhibitor was detected by qPCR. * $p < 0.05$

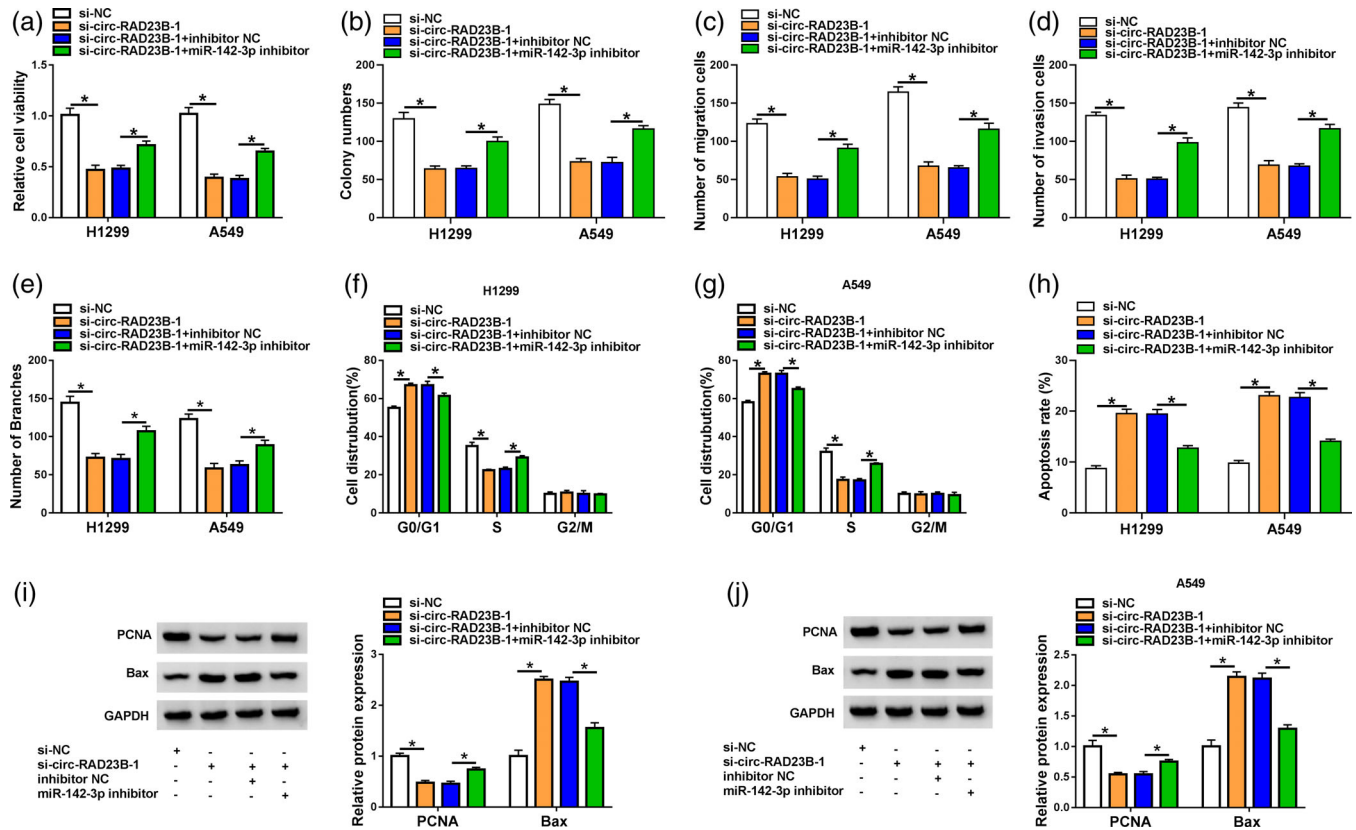


FIGURE 3 Circ-RAD23B knockdown blocked NSCLC development in vitro by mediating miR-142-3p. In H1299 and A549 cells transfected with si-circ-RAD23B-1 or si-circ-RAD23B-1 + miR-142-3p inhibitor, (a and b) cell proliferation was assessed by CCK-8 assay and colony formation assay. (c and d) Cell migration and cell invasion were assessed by transwell assay. (e) The angiogenic ability was assessed by Matrigel tube formation assay. (f and g) Cell cycle distribution was determined by flow cytometry assay. (h) Cell apoptosis was analyzed by flow cytometry assay. (i and j) The expression of PCNA and Bax was measured by western blot. * $p < 0.05$

reduced luciferase activity in H1299 and A549 transfected with WT-circ-RAD23B but not MUT-circ-RAD23B (Figure 2c). MiR-142-3p expression was remarkably decreased in NSCLC tissues compared to normal tissues, as well as in H1299 and A549 cells compared to 16 HBE cells (Figure 2d and e). MiR-142-3p expression notably declined in H1299 and A549 cells transfected with miR-142-3p inhibitor (Figure 2f). In addition, the expression of miR-142-3p was notably promoted in H1299 and A549 cells transfected with si-circ-RAD23B-1 but repressed in cells transfected with si-circ-RAD23B-1 + miR-142-3p inhibitor (Figure 2g). The data revealed that miR-142-3p was a target of circ-RAD23B.

MiR-142-3p suppression recovered circ-RAD23B knockdown-inhibited cell malignant behaviors in H1299 and A549 cells

In terms of function, si-circ-RAD23B-1-blocked cell viability and colony formation ability were partly recovered miR-142-3p inhibitor (Figure 3a and b). Besides, cell migration and cell invasion were notably suppressed in cells transfected with si-circ-RAD23B-1 but restored in cells

transfected with si-circ-RAD23B-1 + miR-142-3p inhibitor (Figure 3c and d). In addition, angiogenesis was inhibited by circ-RAD23B deficiency but partly recovered by miR-142-3p inhibitor (Figure 3e). Moreover, cell distribution arrested at the G0/G1 phase caused by circ-RAD23B knockdown largely was relieved by miR-142-3p inhibition (Figure 3f and g). For apoptosis, circ-RAD23B knockdown markedly promoted cell apoptosis, while miR-142-3p inhibition partly repressed cell apoptosis (Figure 3h). Additionally, circ-RAD23B knockdown-inhibited PCNA expression was largely recovered by miR-142-3p inhibition, and circ-RAD23B knockdown-enhanced Bax expression was largely depleted by miR-142-3p inhibition (Figure 3i and j). These data manifested that circ-RAD23B knockdown inhibited NSCLC development in vitro by increasing miR-142-3p expression.

MAP4K3 was a target of miR-142-3p

The data from the miCode tool showed that MAP4K3 was one of the targets of miR-142-3p, and miR-142-3p harbored a special binding site with MAP4K3 3'UTR (Figure 4a). In the dual-luciferase reporter assay, we found that miR-

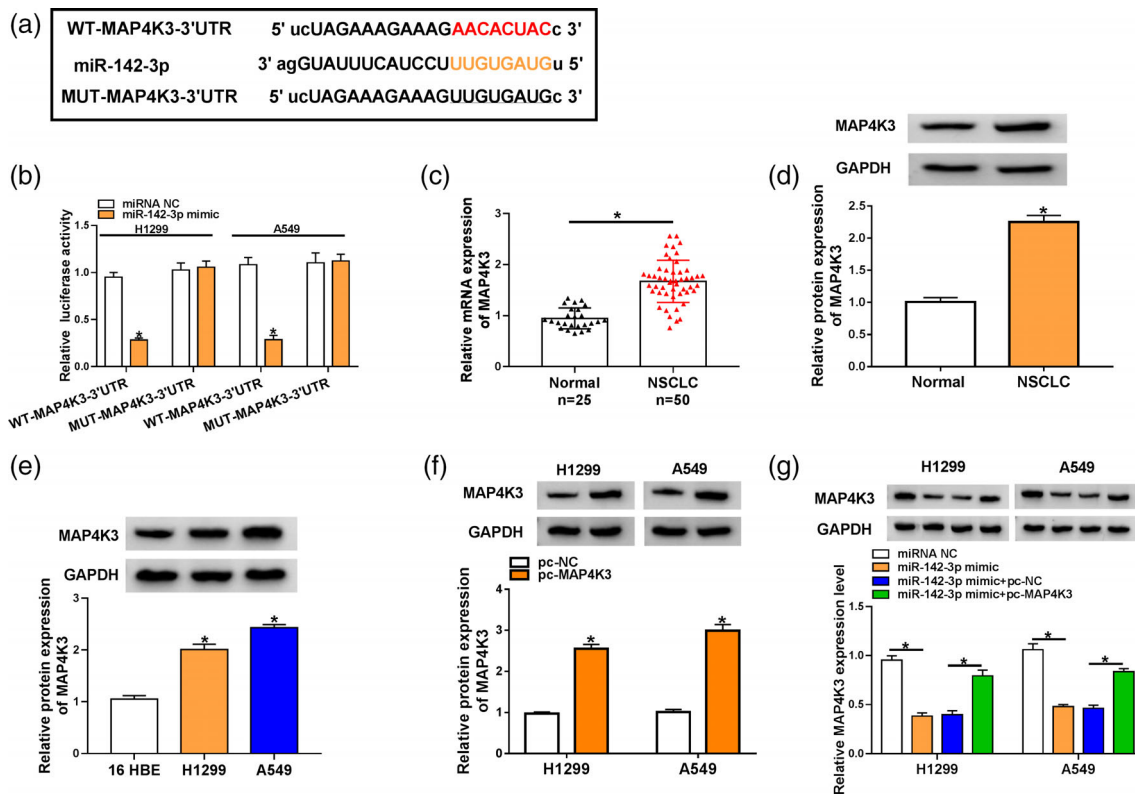


FIGURE 4 MAP4K3 was a target of miR-142-3p. (a) The binding site between MAP4K3 3'UTR and miR-142-3p was provided by miRcode tool. (b) Dual-luciferase reporter assay was conducted to validate the interaction between miR-142-3p and MAP4K3. (c and d) the expression of MAP4K3 in NSCLC tissues and normal tissues was detected by qPCR and western blot. (e) The expression of MAP4K3 protein in H1299, A549 and 16 HBE cells was measured by western blot. (f) The efficiency of MAP4K3 overexpression was checked by western blot. (g) The expression of MAP4K3 in H1299 and A549 cells transfected with miR-142-3p mimic or miR-142-3p mimic+pc-MAP4K3 was detected by western blot. * $p < 0.05$

142-3p mimic significantly reduced luciferase activity in H1299 and A549 cells transfected with WT-MAP4K3-3'UTR but not MUT-MAP4K3-3'UTR (Figure 4b). MAP4K3 expression was relatively higher in NSCLC tissues ($n = 50$) than that in normal tissues ($n = 25$) (Figure 4c and d). In addition, MAP4K3 protein expression was increased in H1299 and A549 cells compared with that in 16 HBE cells (Figure 4e). In addition, MAP4K3 protein expression was shown to be notably increased in H1299 and A549 cells transfected with pc-MAP4K3 compared to pc-NC (Figure 4f). We then monitored that MAP4K3 protein expression was strikingly decreased in H1299 and A549 cells transfected with miR-142-3p mimic but recovered in cells transfected with miR-142-3p mimic +pc-MAP4K3 (Figure 4g). These data showed that miR-142-3p regulated MAP4K3 expression by binding to MAP4K3 3'UTR.

MiR-142-3p degraded the function of MAP4K3

In functional analyses, we found that miR-142-3p mimic significantly weakened cell viability and colony formation ability, while MAP4K3 reintroduction rescued these inhibitory effects (Figure 5a and b). In addition, cell migration

and cell invasion were markedly suppressed by miR-142-3p restoration but partly recovered by MAP4K3 reintroduction (Figure 5c and d). The number of branches in HUVECs was depleted by miR-142-3p restoration but partly enhanced by MAP4K3 overexpression (Figure 5e). In addition, miR-142-3p mimic induced cell cycle arrest at the G0/G1 phase, while MAP4K3 overexpression alleviated this arrest (Figure 5f and g). Cell apoptosis promoted by miR-142-3p enrichment was also repressed by the reintroduction of MAP4K3 (Figure 5h). Additionally, miR-142-3p restoration-suppressed PCNA expression was partly restored by MAP4K3 reintroduction, and miR-142-3p restoration-strengthened Bax expression was partly repressed by MAP4K3 reintroduction (Figure 5i and j). These data suggested that miR-142-3p targeted MAP4K3 to block NSCLC development in vitro.

Circ-RAD23B/miR-142-3p/MAP4K3 axis regulated the MAPK signaling pathway

Subsequent experiments demonstrated that MAP4K3 protein expression was notably decreased in H1299 and A549 cells transfected with si-circ-RAD23B-1 compared to si-NC, while MAP4K3 expression was partly increased in cells

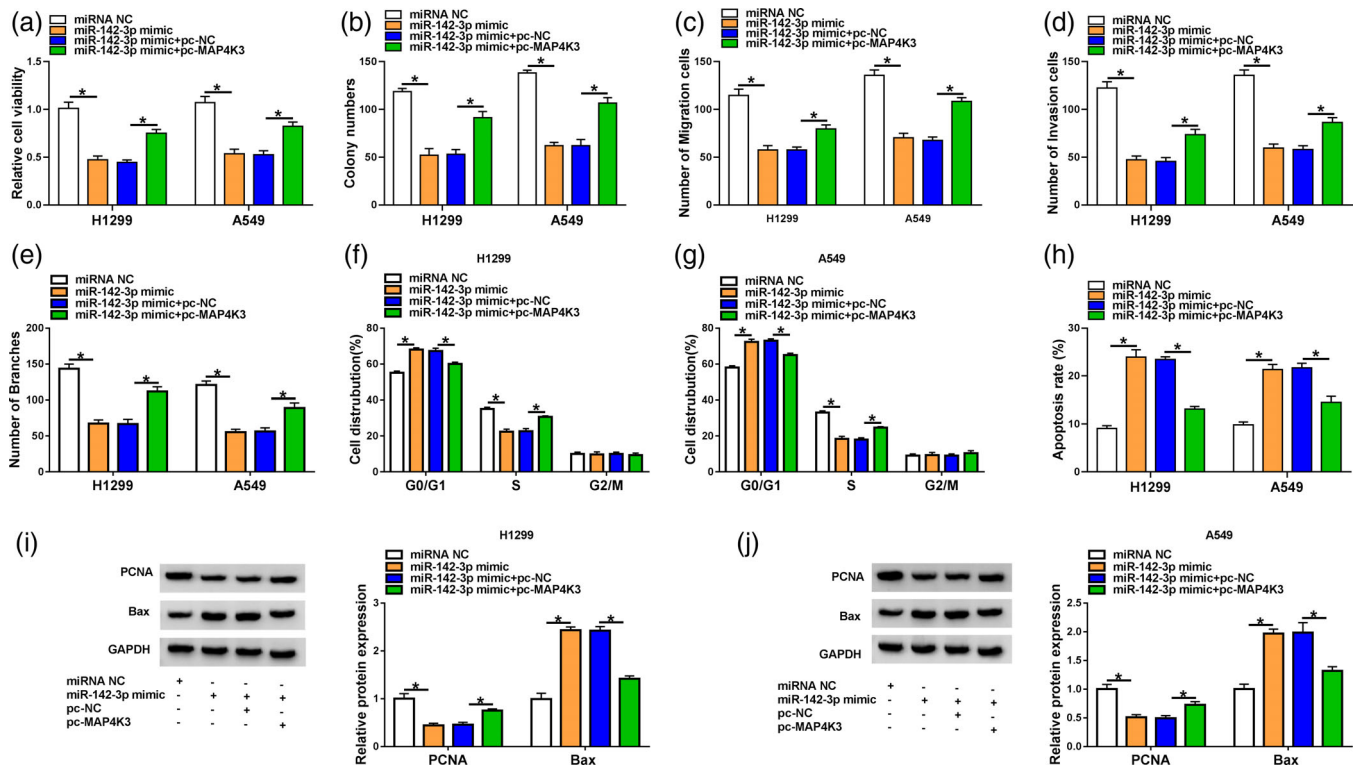


FIGURE 5 MiR-142-3p blocked NSCLC development in vitro by depleting MAP4K3. In H1299 and A549 cells transfected with miR-142-3p mimic or miR-142-3p mimic+pc-MAP4K3, (a and b) cell proliferation was assessed by CCK-8 assay and colony formation assay. (c and d) cell migration and cell invasion were assessed by transwell assay. (e) The angiogenic ability was investigated by Matrigel tube formation assay. (f and g) Cell cycle distribution was determined by flow cytometry assay. (h) Cell apoptosis was investigated by flow cytometry assay. (i and j) The expression of PCNA and Bax was detected by western blot. **p* < 0.05

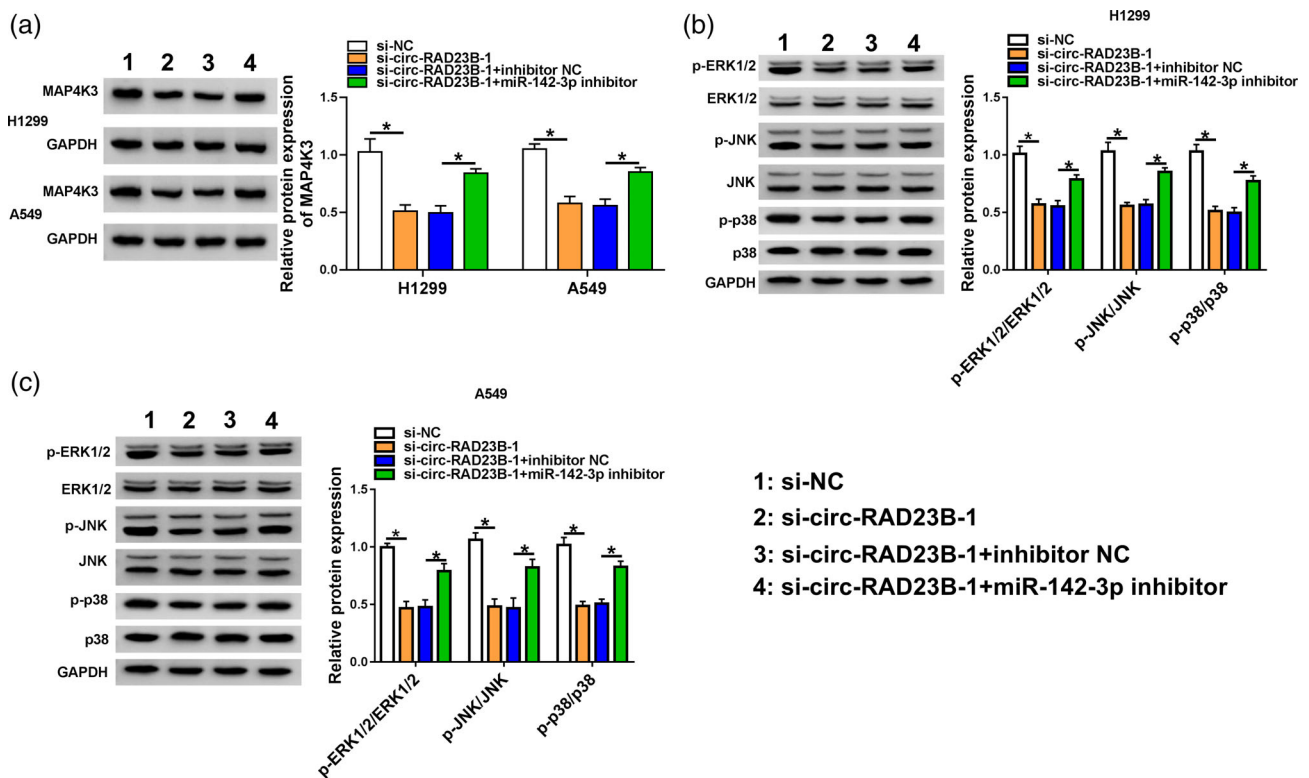


FIGURE 6 The circ-RAD23B/miR-142-3p/MAP4K3 axis regulated the MAPK signaling pathway. (a) The protein level of MAP4K3 in H1299 and A549 cells transfected with si-circ-RAD23B-1 or si-circ-RAD23B-1 + miR-142-3p inhibitor was detected by western blot. (b and c) The protein levels of p-ERK1/2, p-JNK and p-p38 in H1299 and A549 cells transfected with si-circ-RAD23B-1 or si-circ-RAD23B-1 + miR-142-3p inhibitor was detected by western blot. **p* < 0.05

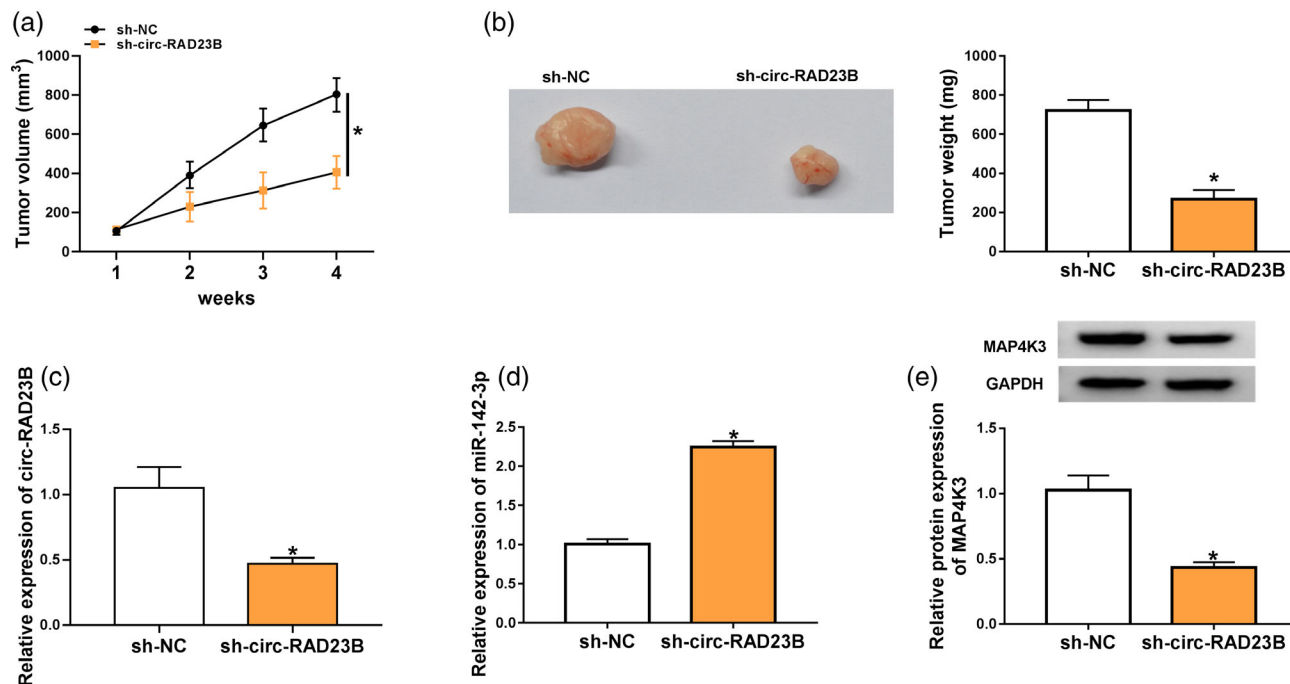


FIGURE 7 Circ-RAD23B knockdown inhibited tumor growth in vivo. In sh-circ-RAD23B or sh-NC-administered mice, (a) tumor volume was measured once a week. (b) Once tumor tissues were excised, tumor size was photographed, and tumor weight was measured. (c and d) The expression of circ-RAD23B and miR-142-3p in the excised tumor tissues was detected by qPCR. (e) The expression of MAP4K3 in the excised tumor tissues was detected by western blot. * $p < 0.05$

transfected with si-circ-RAD23B-1 + miR-142-3p inhibitor compared to si-circ-RAD23B-1 + inhibitor NC (Figure 6a), suggesting that circ-RAD23B regulated MAP4K3 expression by targeting miR-142-3p. Additionally, MAPKs played indispensable roles in numerous signaling pathways, and ERK1/2, JNK and p38 were major groups of MAPKs. Here, we found that the protein levels of p-ERK1/2, p-JNK and p-p38 were strikingly lessened in H1299 and A549 cells transfected with si-circ-RAD23B-1 but partly recovered in cells transfected with si-circ-RAD23B-1 + miR-142-3p inhibitor (Figure 6b and c), suggesting that circ-RAD23B knockdown mediated the inactivation of MAPK signaling pathway by targeting the miR-142-3p/MAP4K3 axis.

Circ-RAD23B knockdown impeded solid tumor growth in mice

In animal models, we found that circ-RAD23B knockdown inhibited tumor growth, leading to smaller tumor volume and tumor weight, and the representative image of tumor nodes showed that circ-RAD23B knockdown produced small tumor size (Figure 7a and b). We performed expression analyses using excised tumor tissues. The results showed that the expression of circ-RAD23B and MAP4K3 protein was strikingly decreased, while the expression of miR-142-3p was increased in tumor tissues excised from sh-circ-RAD23B-administered mice compared to sh-NC (Figure 7c–e). The data showed that circ-RAD23B

knockdown impeded solid tumor growth in vivo by targeting the miR-142-3p/MAP4K3 axis.

DISCUSSION

NSCLC is an aggressive disorder with universal poor survival.¹⁴ Identifying promising biomarkers and novel targets for the effective diagnosis and treatment of NSCLC is urgently required. In this study, we obtained circ-RAD23B from a previous circRNA expression profile and verified high circ-RAD23B expression in NSCLC tissues and cells. Knockdown of circ-RAD23B inhibited NSCLC development by in vitro and in vivo assays. Mechanism analysis found that circ-RAD23B regulated NSCLC progression by modulating the miR-142-3p/MAP4K3 axis. Moreover, the MAPK signaling pathway was inactivated by circ-RAD23B knockdown. Our findings provide evidence for circ-RAD23B as a promising biomarker in NSCLC.

Circ-RAD23B was originally identified to be upregulated in NSCLC tissues by sequencing technology,⁷ which was verified in clinical specimens and cell lines by qPCR. Recently, circ-RAD23B high expression was demonstrated to be associated with poor prognosis of NSCLC, and circ-RAD23B depletion significantly restrained cell viability, migration and invasion.¹⁵ Consistent with these data, our study determined that circ-RAD23B knockdown not only suppressed NSCLC cell proliferation, migration and invasion but also promoted cell apoptosis and cell cycle arrest.

Angiogenesis deregulation is regarded to be the main driving force in multiple human diseases including cancers.¹⁶ Angiogenesis produces new tubes that deliver oxygen and nutrients to growing tumor tissues, and thus the blockage of tumor angiogenesis is served as a clinical antitumor strategy.¹⁶ We found that circ-RAD23B knockdown strikingly inhibited the number of tube branches, suggesting that circ-RAD23B inhibited angiogenesis. Moreover, circ-RAD23B downregulation impeded tumor growth in animal models. Overall, all these findings demonstrated that circ-RAD23B knockdown had forceful potency to block NSCLC deterioration.

Accumulating studies have proposed that circRNA participated in cancer progression by competing for miRNAs with downstream mRNAs.^{17–19} In this study, we screened miR-142-3p as a target of circ-RAD23B. Previous studies have illustrated that miR-142-3p overexpression promoted chemosensitivity in NSCLC by targeting high mobility group box-1 (HMGB1).²⁰ In addition, miR-142-3p expression was decreased in NSCLC tissues, and miR-142-3p upregulation inhibited NSCLC cell proliferation, migration and invasion.^{11,21} Consistent with these findings, our data presented that miR-142-3p restoration suppressed NSCLC cell proliferation, migration, invasion and angiogenesis. Rescue experiments discovered that miR-142-3p inhibition reversed the effects of circ-RAD23B knockdown, suggesting that circ-RAD23B knockdown blocked NSCLC progression by increasing miR-142-3p expression.

We next defined that MAP4K3 was a target of miR-142-3p. MAP4K3 was previously demonstrated to be an oncogene in NSCLC, and the restoring expression of MAP4K3 enhanced cell migration and invasion.^{22,23} High expression of MAP4K3 was correlated with a high risk of NSCLC recurrence and poor recurrence-free survival rate.¹³ In this study, we proposed that the oncogenic effect of MAP4K3 was suppressed by miR-142-3p because MAP4K3 overexpression recovered the effects of miR-142-3p restoration in rescue experiments. Given that MAP4K3 is a member of the MAP4K family, we speculated that MAP4K3 might be involved in the MAPK signaling pathway. MAPKs are major signaling transduction molecules with vital functions in regulating a variety of cellular responses, such as cell proliferation, differentiation and apoptosis.²⁴ ERK1/2, JNK and p38 are main compounds of MAPKs, which are closely involved in the regulation of various cancer cell activities, including proliferation, apoptosis and metastasis.^{25,26} Sun et al. illustrated that the phosphorylation of ERKs, JNK and p38 was increased in bladder cancer cells compared to non-cancer cells.²⁷ Zhou et al. reported that MRS1754 (a selective A2b receptor antagonist) treatment significantly inhibited tumor growth of bladder urothelial carcinoma and degraded the phosphorylation levels of ERKs, JNK and p38.²⁸ Gao et al. stated that miR-9 inhibition suppressed osteosarcoma cell proliferation by depleting the phosphorylation levels of ERKs, JNK and p38.²⁹ Herein, consistent with these views, our data revealed that circ-RAD23B knockdown reduced the phosphorylation levels of ERK1/2,

JNK and p38, while miR-142-3p inhibition recovered their levels, suggesting that circ-RAD23B regulated the MAPKs signaling pathways in NSCLC.

In conclusion, our study mainly clarified that circ-RAD23B was highly expressed in NSCLC tissues and cells. Knockdown of circ-RAD23B inhibited NSCLC cell malignant behaviors, including proliferation, migration, invasion, angiogenesis and cell cycle progression, and also blocked tumor growth in vivo. Circ-RAD23B conducted these effects by regulating the miR-142-3p/MAP4K3 axis. Moreover, the deregulation of MAPK signaling pathway might be involved in the circ-RAD23B regulatory networks. Our data strongly support that circ-RAD23B is a promising therapeutic target of NSCLC.

ACKNOWLEDGEMENTS

This study was supported by the Natural Science Foundation of Fujian Province [2018J01274].

CONFLICT OF INTEREST

The authors declare that they have no financial conflicts of interest.

ORCID

Yunjian Huang  <https://orcid.org/0000-0003-3064-6067>

REFERENCES

1. Siegel RL, Miller KD, Jemal A. Cancer statistics, 2019. *CA Cancer J Clin.* 2019;69(1):7–34.
2. Yang CY, Yang JC, Yang PC. Precision Management of Advanced Non-Small Cell Lung Cancer. *Annu Rev Med.* 2020;71:117–36.
3. Chen L, Nan A, Zhang N, Jia Y, Li X, Ling Y, et al. Circular RNA 100146 functions as an oncogene through direct binding to miR-361-3p and miR-615-5p in non-small cell lung cancer. *Mol Cancer.* 2019;18(1):13.
4. Jiang MM, Mai ZT, Wan SZ, Chi YM, Zhang X, Sun BH, et al. Microarray profiles reveal that circular RNA hsa_circ_0007385 functions as an oncogene in non-small cell lung cancer tumorigenesis. *J Cancer Res Clin Oncol.* 2018;144(4):667–74.
5. Li C, Zhang L, Meng G, Wang Q, Lv X, Zhang J, et al. Circular RNAs: pivotal molecular regulators and novel diagnostic and prognostic biomarkers in non-small cell lung cancer. *J Cancer Res Clin Oncol.* 2019; 145(12):2875–89.
6. Zhao J, Li L, Wang Q, Han H, Zhan Q, Xu M. CircRNA expression profile in early-stage lung adenocarcinoma patients. *Cell Physiol Biochem.* 2017;44(6):2138–46.
7. Zhang S, Zeng X, Ding T, Guo L, Li Y, Ou S, et al. Microarray profile of circular RNAs identifies hsa_circ_0014130 as a new circular RNA biomarker in non-small cell lung cancer. *Sci Rep.* 2018;8(1):2878.
8. Ebert MS, Neilson JR, Sharp PA. MicroRNA sponges: competitive inhibitors of small RNAs in mammalian cells. *Nat Methods.* 2007; 4(9):721–6.
9. Memczak S, Jens M, Elefsinioti A, Torti F, Krueger J, Rybak A, et al. Circular RNAs are a large class of animal RNAs with regulatory potency. *Nature.* 2013;495(7441):333–8.
10. Sumazin P, Yang X, Chiu HS, Chung WJ, Iyer A, Llobet-Navas D, et al. An extensive microRNA-mediated network of RNA-RNA interactions regulates established oncogenic pathways in glioblastoma. *Cell.* 2011;147(2):370–81.
11. Liu J, Tian W, Zhang W, Jia Y, Yang X, Wang Y, et al. MicroRNA-142-3p/MALAT1 inhibits lung cancer progression through repressing beta-catenin expression. *Biomed Pharmacother.* 2019;114:108847.

12. Chen DY, Chuang HC, Lan JL, Chen YM, Hung WT, Lai KL, et al. Germinal center kinase-like kinase (GLK/MAP4K3) expression is increased in adult-onset Still's disease and may act as an activity marker. *BMC Med.* 2012;10:84.
13. Hsu CP, Chuang HC, Lee MC, Tsou HH, Lee LW, Li JP, et al. GLK/MAP4K3 overexpression associates with recurrence risk for non-small cell lung cancer. *Oncotarget.* 2016;7(27):41748–57.
14. Alshangiti A, Chandhoke G, Ellis PM. Antiangiogenic therapies in non-small-cell lung cancer. *Curr Oncol.* 2018;25(Suppl 1):S45–58.
15. Li L, Wan K, Xiong L, Liang S, Tou F, Guo S. CircRNA hsa_circ_0087862 acts as an oncogene in non-small cell lung cancer by targeting miR-1253/RAB3D Axis. *Onco Targets Ther.* 2020;13:2873–86.
16. Wang Z, Dabrosin C, Yin X, Fuster MM, Arreola A, Rathmell WK, et al. Broad targeting of angiogenesis for cancer prevention and therapy. *Semin Cancer Biol.* 2015;35(Suppl):S224–S43.
17. Yu C, Cheng Z, Cui S, Mao X, Li B, Fu Y, et al. circFOXO1 promotes proliferation of non-small cell lung carcinoma cells by acting as a ceRNA to upregulate FAM83D. *J Exp Clin Cancer Res.* 2020;39(1):55.
18. Chen T, Yang Z, Liu C, Wang L, Yang J, Chen L, et al. Circ_0078767 suppresses non-small-cell lung cancer by protecting RASSF1A expression via sponging miR-330-3p. *Cell Prolif.* 2019;52(2):e12548.
19. Xue M, Hong W, Jiang J, Zhao F, Gao X. Circular RNA circ-LDLRAD3 serves as an oncogene to promote non-small cell lung cancer progression by upregulating SLC1A5 through sponging miR-137. *RNA Biol.* 2020;17(12):1811–22.
20. Chen Y, Zhou X, Qiao J, Bao A. MiR-142-3p overexpression increases chemo-sensitivity of NSCLC by inhibiting HMGB1-mediated autophagy. *Cell Physiol Biochem.* 2017;41(4):1370–82.
21. Jin C, Xiao L, Zhou Z, Zhu Y, Tian G, Ren S. MiR-142-3p suppresses the proliferation, migration and invasion through inhibition of NR2F6 in lung adenocarcinoma. *Hum Cell.* 2019;32(4):437–46.
22. Zhao B, Han H, Chen J, Zhang Z, Li S, et al. MicroRNA let-7c inhibits migration and invasion of human non-small cell lung cancer by targeting ITGB3 and MAP4K3. *Cancer Lett.* 2014;342(1):43–51.
23. Wang Z, Han Z, Zhang L, Zhang S, Wang B. MicroRNA-98-5p regulates the proliferation and apoptosis of A549 cells by targeting MAP4K3. *Oncol Lett.* 2019;18(4):4288–93.
24. Chuang HC, Wang X, Tan TH. MAP4K family kinases in immunity and inflammation. *Adv Immunol.* 2016;129:277–314.
25. Wang C, Zhang X, Zhang C, Zhai F, Li Y, Huang Z. MicroRNA-155 targets MAP3K10 and regulates osteosarcoma cell growth. *Pathol Res Pract.* 2017;213(4):389–93.
26. Gui ZL, Wu TL, Zhao GC, Lin ZX, Xu HG. MicroRNA-497 suppress osteosarcoma by targeting MAPK/Erk pathway. *Bratisl Lek Listy.* 2017;118(8):449–52.
27. Sun M, Zhao W, Chen Z, Li M, Li S, Wu B, et al. Circular RNA CEP128 promotes bladder cancer progression by regulating Mir-145-5p/Myd88 via MAPK signaling pathway. *Int J Cancer.* 2019;145(8):2170–81.
28. Zhou Y, Chu X, Yi Y, Hao Z, Zheng X, Yuxin T, et al. MRS1754 inhibits proliferation and migration of bladder urothelial carcinoma by regulating mitogen-activated protein kinase pathway. *J Cell Physiol.* 2019;234(7):11360–8.
29. Gao S, Wang J, Tian S, Luo J. miR9 depletion suppresses the proliferation of osteosarcoma cells by targeting p16. *Int J Oncol.* 2019;54(6):1921–32.

SUPPORTING INFORMATION

Additional supporting information may be found in the online version of the article at the publisher's website.

How to cite this article: Zhuang Q, Huang Z, Zhuang W, Hong Y, Huang Y. Knockdown of circ-RAD23B inhibits non-small cell lung cancer progression via the miR-142-3p/MAP4K3 axis. *Thorac Cancer.* 2022;13:750–60. <https://doi.org/10.1111/1759-7714.14319>